Earth and Planetary Science Letters 289 (2010) 105–111

Contents lists available at ScienceDirect

Earth and Planetary Science Letters

journal homepage: www.elsevier.com/locate/epsl

Mantle transition zone beneath the Caribbean-South American plate boundary and its tectonic implications

Jianping Huang [a,b], Elizabeth Vanacore [a], Fenglin Niu [a,*], Alan Levander [a]

[a] Department of Earth Science, MS-126, Rice University, 6100 Main St., Houston, TX 77005, USA
[b] College of Geo-Resources and Information, China University of Petroleum, Qingdao, China

ARTICLE INFO

Article history:
Received 27 March 2009
Received in revised form 17 October 2009
Accepted 25 October 2009
Available online 5 December 2009

Edited by: R.D. van der Hilst

Keywords:
Mantle discontinuities
phase transition
receiver function
Lesser Antilles subduction zone
slab detachment

ABSTRACT

We analyzed receiver-function data recorded by a temporary broadband array deployed as part of the BOLIVAR project and the permanent seismic network of Venezuela to study the mantle transition zone structure beneath the Caribbean-South American plate boundary and Venezuela. Significant topography on both the 410-km and the 660-km discontinuities was clearly imaged in the CCP (common-conversion-point) stacked images. Beneath the southeastern Caribbean, the 410-km is featured by a narrow (~200 km EW) ~25-km uplift extending in the NS direction around 63° west, while the 660-km is depressed by ~20 km in a narrow region slightly west to the uplift, a scenario that is more consistent with westward descent of the oceanic South American plate rather than a break-off of NNW dipping proto-Caribbean oceanic lithosphere along the El Pilar Fault. We also found a thick transition zone beneath the Falcon region in northwestern Venezuela, possibly associated with the subducted Nazca plate. A flat 410-km was observed beneath the Guayana shield, suggesting that the shield has a stable and moderately deep keel, which has little effect on the underlying transition zone structure.

1. Introduction

The southeastern Caribbean plate is bounded to the east by the Antilles subduction zone, where the Atlantic part of the South American (SA) plate subducts beneath the Caribbean, and to the south by the El-Pilar-San Sebastian transform fault system. The Caribbean plate (CAR) is moving eastward relative to the stable SA plate since late Paleocene (Burke, 1988) with a current velocity of ~20 mm/yr (e.g., Pérez et al., 2001). This relative motion of the two plates resulted in a progressive west-to-east detachment of the Atlantic lithosphere from the continental SA plate at the southern edge of the subduction zone. However, it is still unclear whether the detachment has a hinge geometry (e.g., Govers and Wortel, 2005; Clark et al., 2008) or a tensile geometry (e.g., VanDecar et al., 2003) (Fig. 1). The hinge or shear tear model predicts a simple subduction geometry of the Atlantic lithosphere along the Antilles arc, while the latter involves tearing the proto-Caribbean oceanic lithosphere that results in a curtain of oceanic lithosphere dangling beneath the northern edge of the South American continent. The tensile tear model thus predicts a more complicated geometry of the subducted oceanic lithosphere in the mantle than the shear tear model. Mapping the subducted oceanic lithosphere beneath the southeastern CAR plate provides an important line of evidence for understanding the regional tectonics.

In principle, the subducted cold oceanic lithosphere can be imaged by seismic tomography as distinct high-velocity anomalies (HVAs). As schematically shown in Fig. 1, the shape and location of the HVAs associated with the subducting plate in the upper mantle are expected to be very different between the two models. At each depth, the subducting slab in the shear tear model would produce an elongated thermal and velocity anomaly extending roughly in the north-south direction. On the other hand, the slab geometry in the tensile model is more complicated. It consists of a component that extends in the east-west direction and is located right beneath the northern edge of South America. While global tomography models (e.g., van der Hilst et al., 1997, Fukao et al., 2001; Grand, 2002) did show high velocity anomalies extending at least to the transition zone depths, the lateral resolution (~500 km) of these models is not enough to distinguish between the two tear models. On the other hand, the existing regional models (e.g., van der Hilst and Mann, 1994; VanDecar et al., 2003) are somehow too local to cover the broad area of the CAR-SA plate boundary, largely due to the poor coverage of seismic stations in the region.

The 410-km and 660-km seismic discontinuities that bound the mantle transition zone are believed to be caused by temperature-sensitive phase transitions from olivine α-$(Mg,Fe)_2SiO_4$ to wadsleyite β-$(Mg,Fe)_2SiO_4$ (Katsura and Ito, 1989) and from ringwoodite γ-$(Mg,Fe)_2SiO_4$ to perovskite $(Mg,Fe)SiO_3$ plus magnesiowüstite $(Mg,Fe)O$ (Ito and Takahashi, 1989), respectively. The latter is also known as the post-spinel transformation. Because the two phase-transitions have positive and negative Clapeyron slopes, respectively, a decrease in temperature results in a decrease in the depth to the 410-km

* Corresponding author. Tel.: +1 713 348 6064; fax: +1 713 348 5214.
E-mail address: niu@rice.edu (F. Niu).

0012-821X/$ – see front matter © 2009 Elsevier B.V. All rights reserved.
doi:10.1016/j.epsl.2009.10.033

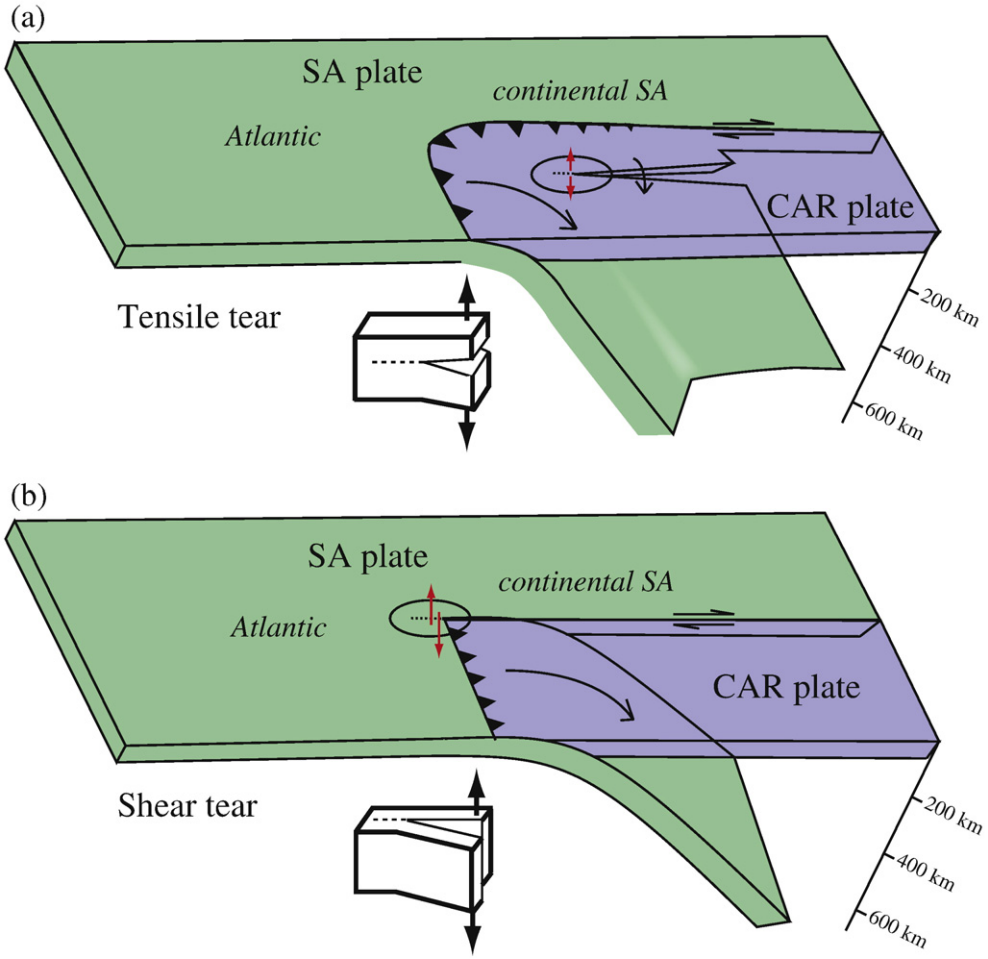

Fig. 1. Schematic diagram showing the tensile (a) and shear (b) tear models proposed for slab detachment occurring at the southeastern CAR-SA plate boundary. Modified from Clark (2008).

discontinuity and an increase in the depth to the 660-km discontinuity. Lateral variations in the transition-zone thickness, as well as variations in the depths of the two discontinuities can be used to indirectly map out a descending slab. Global mapping of the two discontinuities using SS precursor data (e.g., Flanagan and Shearer, 1998) found an up to 20-km depression of the 660-km discontinuity around the Pacific subduction zones. Large depth variations, in the order of 20–70 km, were also observed by numerous high-resolution regional studies with different imaging techniques from various subduction zones around the Pacific (e.g., Vidale and Benz, 1992; Wicks and Richards, 1993; Niu and Kawakatsu, 1995; Collier and Helffrich, 1997; Niu et al., 2005; Li et al., 2008). The global topography map (Flanagan and Shearer, 1998) of the two discontinuities, on the other hand, does not show any anomalies beneath the Antilles subduction. So far, there is no regional study of the two discontinuities beneath the CAR-SA plate boundary.

Until recently, it was generally believed that the origin of the observed topography on the two seismic discontinuities was due to temperature as the calculated Clapeyron slopes from the seismic data are consistent with the experimentally determined Clapeyron slopes, approximately ~2.5 MPa/K for the olivine-wadsleyite (Katsura and Ito, 1989) and ~-3 MPa/K for the post-spinel phase transition (Ito and Takahashi, 1989). Most recent mineral physics studies (Katsura et al., 2003; Fei et al., 2004; Litasov et al., 2005), however, found that the Clapeyron slope of the post-spinel phase transition of anhydrous ringwoodite is rather small, between -2 to -0.4 MPa/K. Litasov et al. (2005) suggested that significant portion of the seismically observed topography might be caused by water content rather than temperature. Since the transition zone minerals, wadsleyite and ringwoodite, have an enhanced water storage capacity over the upper and lower mantle mineral assemblages (e.g., Kohlstedt et al., 1996), the presence of water can expand the stable region of the transition zone minerals, resulting in an uplifted 410-km and depressed 660-km, which has a similar effect to reduced temperature on the two discontinuities (e.g., Wood, 1995; Higo et al., 2001). The competing effects of water and temperature on discontinuity structure make the depth changes in transition zone discontinuities difficult to interpret. Characterizing the depths of the two discontinuities in different subduction zones becomes crucial in resolving whether temperature or water is the cause of the observed topography. As mentioned above, the majority of seismic observations were made around the Pacific subduction zones, making measurements at any other subduction zones valuable.

In this study, we applied receiver function analysis techniques to a large broadband seismic dataset to image the mantle transition-zone structure beneath the CAR-SA plate boundary. Our primary goal is to provide some constraints to the long-standing debate on the style of slab detachment occurring at this boundary. The new dataset and seismic images, on the other hand, also offer insights to our general understanding of the chemistry and thermal state at the base of the upper mantle.

2. Data and Analysis

2.1. BOLIVAR array

We used waveform data collected by the BOLIVAR (Broadband Ocean-Land Investigations of Venezuela and the Antilles arc Region) project

(Levander et al., 2006). At the peak deployment, the BOLIVAR array consists of 84 temporary and permanent broadband stations including 15 ocean bottom seismographs (OBS, Fig. 2), forming a large 2D areal array with an aperture ~1200 km from east to west and ~600 km from north to south (Niu et al., 2007). Station spacing varies from ~10 km in a dense line near 64° west to ~100 km in the western Venezuela, which is covered mainly by the national seismic network of the Venezuelan Foundation for Seismological Research (FUNVISIS).

2.2. Receiver functions

We generated receiver functions from earthquakes at epicentral distances between 30° and 90°. We first rotated the two horizontal components of the seismograms to the radial and transverse components. For the OBS stations, we used the component azimuth determined by Niu et al. (2007). Receiver functions were calculated by a deconvolution of the radial component by the vertical component. We adopted the frequency-domain deconvolution method with a water level of 0.003-0.03 that was determined by the background noise level calculated from a time window before the first arrival (Clayton and Wiggins, 1976; Ammon, 1991). We manually checked all the seismograms from 313 teleseismic events and chose the receiver functions whose vertical components after deconvolution have a well-defined simple pulse. A total of 2376 receiver functions from 112 earthquakes were selected for further analysis (Fig. 2 inset).

2.3. CCP stacking

We first low-pass filtered the receiver functions with a corner frequency of 0.2 Hz. We then applied the common-conversion-point (CCP) stacking technique to the receiver-function data to image the P to S conversion events and their lateral variations beneath the array (e.g., Dueker and Sheehan, 1997; Shen et al., 1998; Niu et al., 2004, 2005). For an assumed conversion depth, d, for each source-receiver pair, we first computed the conversion point and the time moveout of the converted phase *Pds* by ray tracing the *iasp91* velocity model (Kennett and Engdahl, 1991). We further used 3D crustal (Niu et al., 2007) and the whole mantle P-wave velocity model of Fukao et al. (2001) to calculate 3D travel-time anomalies. The S-wave velocity model is made from the P-wave velocity by assuming *iasp91* Vp/Vs ratios. Both the crustal and mantle corrections are on the order of ± 0.5 secs., equivalent to a ± 5 km depth correction to the two discontinuities. We divided the study area (5°N to 12°N, 70°W to 62°W) into a 0.1° by 0.1° grid and used a circular cap with a radius of 1 degree for gathering the receiver functions. There are significant overlaps among the caps. This serves to lowpass filter the topographic relief on the two discontinuities with a corner wavelength roughly equivalent to the size of the caps, approximately 200 km. We stacked receiver functions within each cap using an n^{th}-root stacking method (Muirhead, 1968). We chose $n=4$ to reduce the uncorrelated noise relative to the usual linear stack ($n=1$), recognizing that this suppresses conversions with significant dip away from the horizontal. We varied d from 300 to 800 km in increments of 1 km.

3. Results and Discussion

In Fig. 3, we showed five depth sections of the CCP stacked images along three longitudinal (a-c) and two latitudinal lines (d-e). Both the 410-km and 660-km discontinuities can be identified easily from these sections. In Fig. 4, we showed the depth to the two

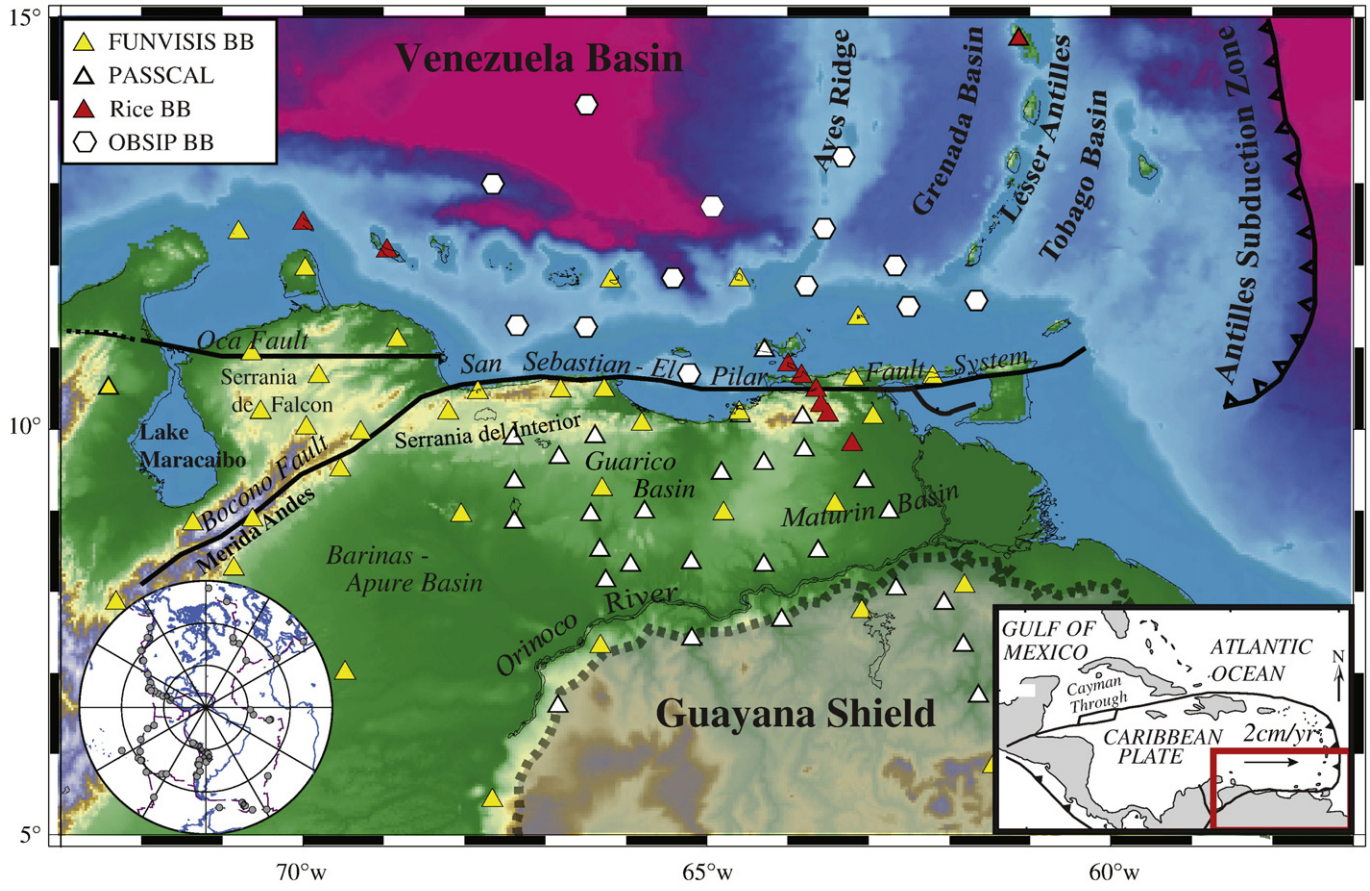

Fig. 2. Map of the southeastern Caribbean and Venezuela. Triangles and hexagons indicate the land and OBS stations, respectively. Major fault systems are also shown in black lines. Inset in the left bottom corner shows the 112 teleseismic events (circles <50 km, diamonds >50 km) used in this study. Inset in the right bottom corner shows the Caribbean plate and surrounding area. Arrow indicates its present motion direction with respect to the stable South America.

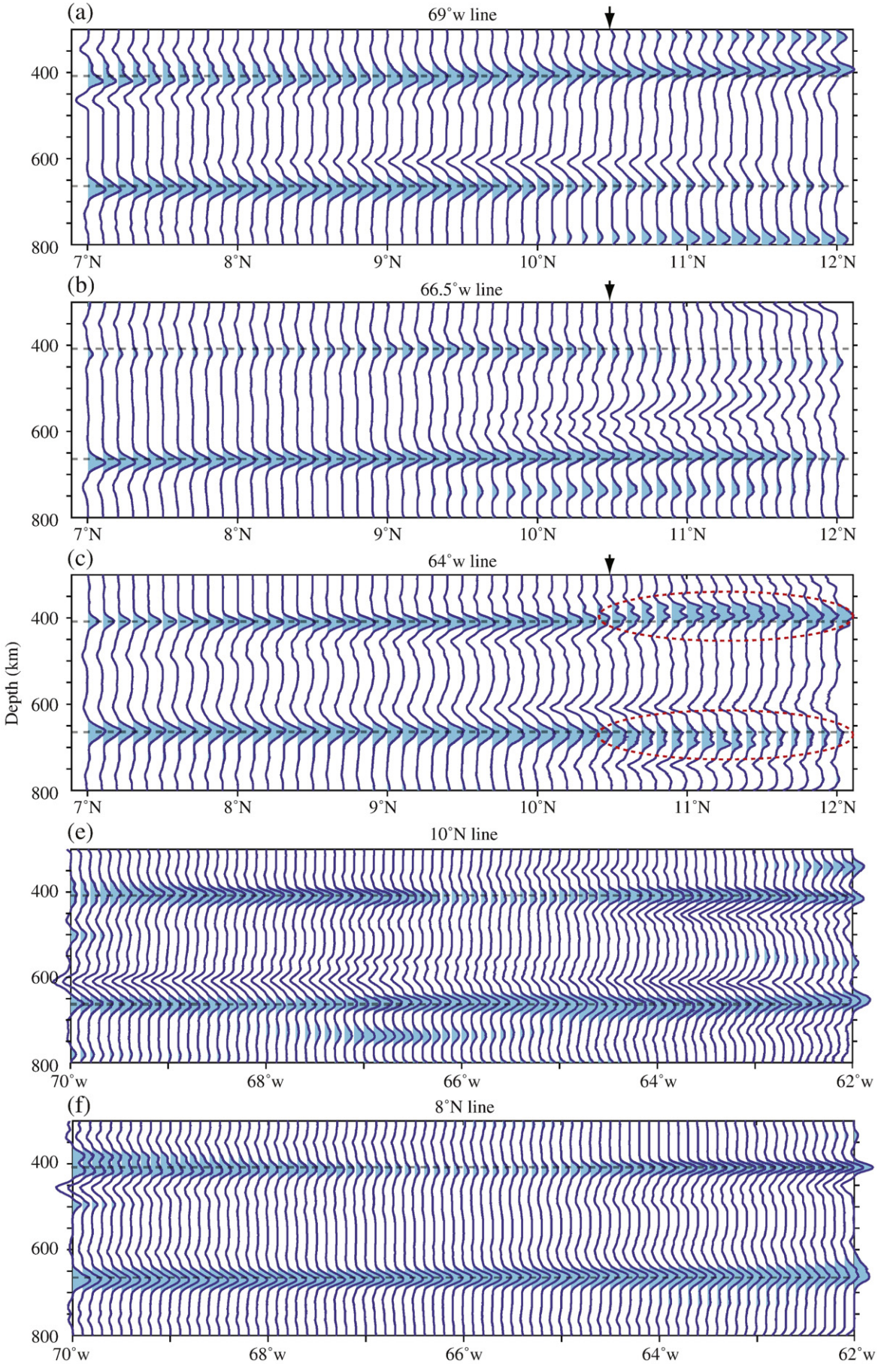
(a)
69°w line
(b)
66.5°w line
(c)
64°w line
Depth (km)
400
600
800
7°N
8°N
9°N
10°N
11°N
12°N
(e)
10°N line
70°w
68°w
66°w
64°w
62°w
(f)
8°N line

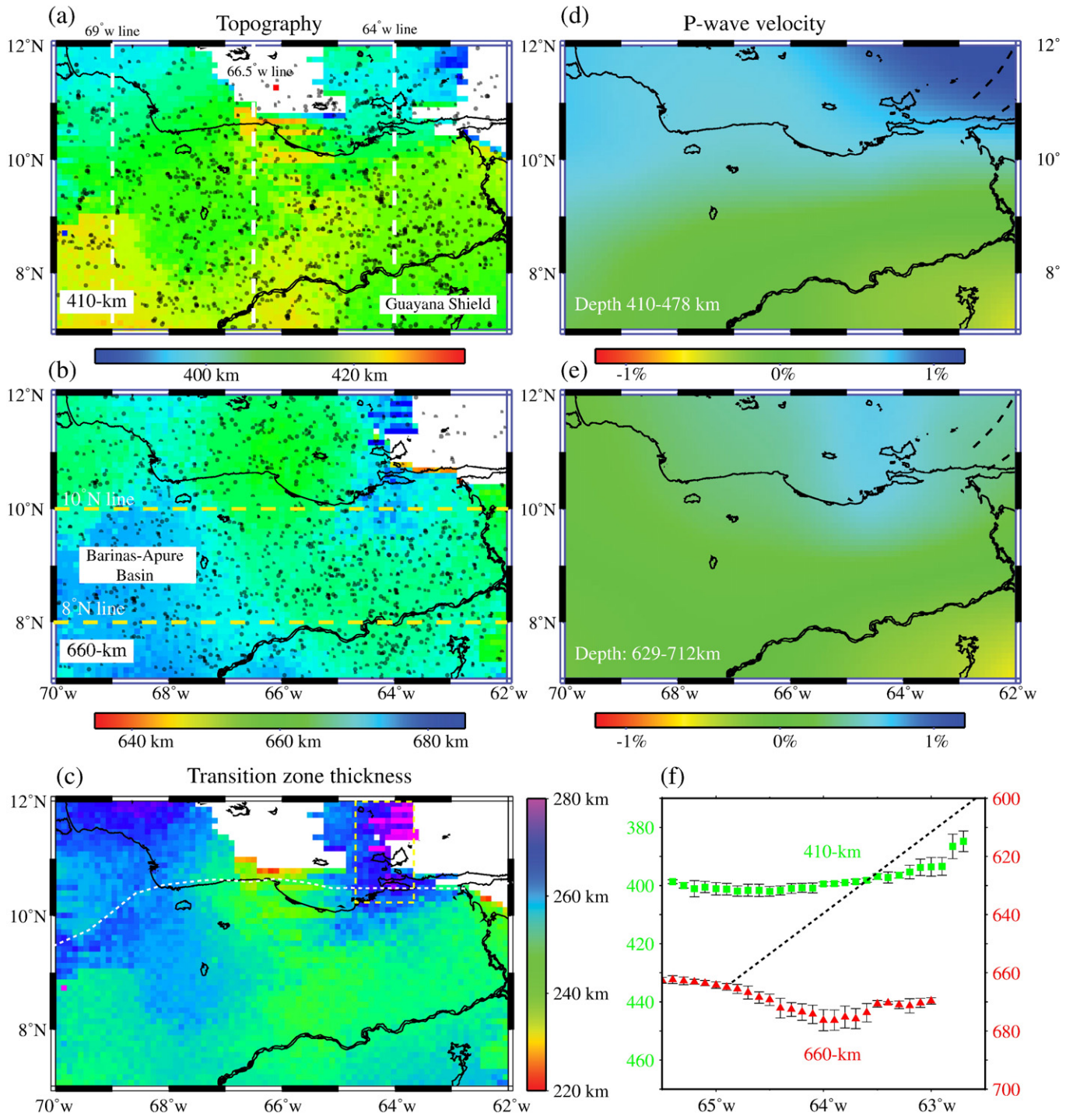

Fig. 4. Map view of (a) the depth to the 410-km discontinuity, (b) the depth to the 660-km discontinuity (b), and (c) mantle transition-zone thickness. P-to-S conversion points are indicated by black dots. P-wave velocity perturbations of Fukao et al. (2001) near the 410 km (d) and 660 km depths (e) are also shown for comparison. Notice the good agreement between the higher velocity anomalies and the uplift of the 410-km and the deepening of the 660-km. (f) Depth of the two discontinuities averaged between 10.5°N-12.0°N is shown as a function of longitude. The depth to the 410-km is indicated in the left and the depth to the 660-km is shown in the right. Dashed line indicates approximately the upper boundary of the subducting Atlantic slab. In general, the observed topography to the two discontinuities and the velocity structure around them agree well with each other except for the southwest corner, where the two discontinuities are about 10 km deeper than the global average while the P-wave velocity appears to be normal. As the transition zone thickness in normal, we speculated that the observed large depths of the two discontinuities beneath the Barinas-Apure Basin are likely caused by the reference model and may not reflect their true depths.

discontinuities and the corresponding transition-zone thickness. In general, we picked the peak of the P-to-S conversion energy as the depth of the two discontinuities. In some regions, the conversion energy spread asymmetrically in a broad depth range and sometime even has multiple peaks. In these cases, we picked the centroid as the event depth. We included 3D structure in calculating the time

Fig. 3. Five depth sections of the CCP gathered receiver functions along three longitudinal and two latitudinal lines. The locations of these sections are shown in Figs. 4a and 4b, respectively. Notice the clear P-to-S conversion from the 410-km and 660-km discontinuities, and large depth variations along the sections. Dashed ellipses indicate the regions with a broad 410-km and 660-km discontinuity.

moveout before the CCP stacking in order to obtain better depth estimates of the two discontinuities. However, since there is no high-resolution velocity model available and our 3D corrections were calculated from global models, it is possible that the depths are biased by unmodeled aspects of the velocity structure of the upper mantle in places. For example, both the 410-km and 660-km are ~10 km deeper beneath the Barinas-Apure Basin (in the left bottom corner of Figs. 4a and b). They are likely to be caused by an unmodeled low S-wave velocity in the upper mantle, as the transition-zone thickness appears to be normal. Because P660s-P410s differential times are not sensitive to heterogeneities shallower than the 410-km discontinuity, the estimated transition-zone thickness is expected to be more accurate than the depths to the individual discontinuities. Our discussion below is therefore based primarily on the observed variations in mantle transition-zone thickness.

The most prominent anomaly in the transition-zone thickness lies beneath the southeastern CAR plate, where we saw a NS-trending anomaly in the transition zone thickness (dashed rectangle) centered at ~64.1° W (Fig. 4c). It is approximately 30 km thicker than the surrounding area and the global average. This thickness anomaly appears to be caused by a ~10 km uplift of the 410-km and a ~20 km depression of the 660-km (Fig. 4e). The maximum topographic relief on the 410-km occurs ~130 km east of the peak depression of the 660-km discontinuity, consistent with a westward subduction geometry of the Atlantic slab. We also found that the topographic anomalies on the two discontinuities agree with the high velocity regions in the global tomographic images (Figs. 4a and d, Figs. 4b and e). The observed topographic anomalies on the two discontinuities extend in the north-south direction, thus it is more consistent with the scenario of a simple westward subduction (Fig. 1b). If a proto-Caribbean lithosphere is detaching from the continental South America (Fig. 1a), then we would also see a topographic anomaly extending in the east-west direction, which is not shown in the CCP stacked images. Along with other lines of seismic evidence, seismicity, crustal structure (Clark et al., 2008), lithosphere structure (Miller et al., 2009), seismic anisotropy (Growdon et al., 2009), we concluded that a shear tear (Fig. 1b) has been occurring in a localized zone between the continental and oceanic segments of the SA plate, and this tear controls the regional tectonics, and results in normal subduction.

As mentioned in the introduction, the origin of a shallower 410-km and a deeper 660-km could be a reduction of temperature, or the presence of water, or both. The sharpness of the two discontinuities has been used to discern the effects of water and temperature (van der Meijde et al., 2003), as the phase transitions occurs in a broader pressure range for an unsaturated hydrous transition zone (e.g., Wood, 1995). We did find that the two discontinuities tend to be broader in the region with a thicker transition zone (dash ellipses in Fig. 3). Although out-of-phase stacking can result in a broad depth distribution of P-to-S conversion energy, we believe that the observe feature of broad discontinuities is likely to be true as they are seen in all the stacked records regardless of the cap size used for stacking. Bina and Helffrich (1994) found that the 410-km becomes broader with decreasing temperature, making it difficult to use the discontinuity sharpness to constrain the origin of the observed 410-km topography. Vacher et al. (1998) found that in a cold environment the breakdown of olivine and garnet appears to occur at different depths, resulting in a broader and complicated boundary between the upper and the lower mantle. The broad 660-km observed here thus does not necessary require a water origin of the depression.

The ~20 km depression of the 660 beneath the southeastern CAR plate is much smaller than those observed in the western and southwestern Pacific subduction zones. Niu and Kawakatsu (1995) found the discontinuity deepens as much as 70 km beneath the Tonga subduction zone. Wicks and Richards (1993) observed a 60 km depression in the discontinuity beneath the Izu-Bonin subduction zone. Both regions are characterized by fast subduction (v) of an old oceanic lithosphere (t) with a steep descending angle (δ), and thus have a very high thermal parameter ($\phi = tv \sin\delta$) (Kirby et al., 1996). Since the Atlantic lithosphere subducting at the Lesser Antilles arc has a low descending rate, and subsequently has a low thermal parameter, we thus expect the subducted Atlantic slab to be less cold than the subducted Pacific slab beneath Tonga and Izu-Bonin arcs. This might explain the low amplitude of the depression observed here. We thus speculate that the primary cause of the depth variations of the two discontinuities beneath the southeastern CAR plate is a temperature reduction. Assuming a wet Clapeyron slope of -3.0 to -2.0 MPa/K (Bina and Helffrich, 1994), we obtained a 222-333 K decrease of temperature within the subducted Atlantic lithosphere.

We also found that the 410-km is shallowing toward the west at the CAR-SA plate boundary (Fig. 4a), resulting in a thicker-than-normal transition zone beneath the northwestern Venezuela (Fig. 4c). On the other hand, the 660-km seems to be normal in the region (Fig. 4b). This feature also matches the tomographic images, which has an elevated velocity around the 410-km but a normal velocity structure at the upper-lower mantle boundary. van der Hilst and Mann (1994) found the upper mantle in this region is rather complicated in their large-scale tomographic model. They interpreted a southeast dipping high-velocity structure as the subduction of the CAR plate underneath the SA plate. The subducting CAR plate extends roughly to the Merida Andes beneath the Bocono Fault, which exhibits a similar geometry to the topographic anomaly on the 410-km (Fig. 4c). But according to van der Hilst and Mann (1994), the CAR plate descends only to 275 km deep, thus it should have little effect on the underlying transition zone structure. van der Hilst and Mann (1994) also found that the Nazca plate is subducting underneath the CAR plate to a depth of ~500 km in the region. The subducting Nazca plate in the region thus could be the cause of the elevated 410-km observed here.

The 410-km and the 660-km discontinuities, on the other hand, are very flat beneath the Guayana craton. The depth extend of cratons has been extensively debated for many decades (e.g., Lerner-Lam and Jordan, 1987; Polet and Anderson, 1995), and the 410-km topography has been used to constrain this depth as the thermal effect of a thick cratonic keel should result in an elevated 410-km (e.g., Li et al., 1998, Niu et al., 2004). Niu et al. (2004) further argued that a flat 410-km could also place a low bound (~160 km) on the depth of the lithosphere beneath a craton. When the lithosphere is thin, a thick and unstable thermal layer forms below the lithosphere, which could eventually develop into a downwelling and deflect the 410-km. On the other hand, a very thick keel (≥~370 km) could post direct thermal effects on the 410-km discontinuity. Our observation of a flat 410-km beneath the Guayana shield thus suggests that the shield has a stable and moderately deep root (between ~160 and ~370 km).

4. Conclusions

We investigated the mantle transition zone structure beneath the CAR-SA plate boundary with receiver function data recorded by the BOLIVAR passive seismic array. The new seismic images allow us to reach the following three conclusions. (1) Beneath the southeastern CAR plate, the subducted Atlantic slab can be traced from the topographic anomalies on the 410-km and 660-km discontinuities. The slab is subducting toward the west at the Lesser Antilles arc and uplifts the 410-km up to ~25 km as it enters the transition zone at around 63.5°W (beneath the Aves Ridge). It also depresses the 660-km by as much as ~20 km when it runs into the upper and lower mantle at around 65°W (beneath the Venezuela Basin). Both the uplift and depression are elongated in the NS direction, suggesting that there is little evidence for a west-to-east progressive tensile tear of the pro-Caribbean oceanic lithosphere originally attached to the northern edge of the continental SA plate. (2) We found an elevated 410-km beneath

the Maracaibo block at the western end of CAR-SA boundary in Venezuela. Based on published tomographic images, we interpret it as evidence for the subducting Nazca plate. (3) We saw a flat 410-km beneath the Guayana shield. The lithosphere beneath the shield must be moderately thick and stable so it does little to the underlying transition zone.

Acknowledgments

We thank FUNVISIS for providing access to their new digital broadband data as part of this collaboration. We would like to thank Gary Pavlis, Frank Vernon, Herbert Rendon, Michael Schmitz and many other BOLIVAR/GEODINOS field personnel for collecting the high quality data. We thank Stoney Clark for providing the schematic diagram of the tensile and shear models, which is the base of Fig. 1. Critical comments from two anonymous reviewers significantly improved the quality of this paper. The BOLIVAR project was funded by the NSF grants EAR-0003572 and EAR-0607801. J.H. was supported by the scholarship of the China Scholarship Council. F.N. is supported by NSF grant EAR-0748455. F.N. expresses special thanks to Rice University for the generous support to his fieldwork in Venezuela.

References

Ammon, C.J., 1991. The isolation of receiver effects from teleseismic P waveforms. Bull. Seismol. Soc. Am. 81, 2504–2510.
Bina, C.R., Helffrich, G., 1994. Phase transition Clapeyron slopes and transition zone seismic discontinuity topography. J. Geophys. Res. 99, 15853–15860.
Burke, K., 1988. Tectonic evolution of the Caribbean. Ann. Rev. Earth Planet. Sci. 16, 201–230.
Clark, S.A., 2008 Characterizing the southeast Caribbean - South American plate boundary at 64°W, Ph.D. thesis, Rice University, 74 p.
Clark, S.A., Sobiesiak, M., Zelt, C.A., Magnani, M.B., Miller, M.S., Bezada, M.J., Levander, A., 2008. Identification and tectonic implications of a tear in the South American plate at the southern end of the Lesser Antilles. Geochem. Geophys. Geosyst. 9, Q11004. doi:10.1029/2008GC002084.
Clayton, R.W., Wiggins, R.A., 1976. Source shape estimation and deconvolution of teleseismic body waves. Geophys. J. R. Astron. Soc. 47, 151–177.
Collier, J., Helffrich, G., 1997. Topography of the "410" and "660" km seismic discontinuities in the Izu-Bonin subduction zone. Geophys. Res. Lett. 24, 1535–1538.
Dueker, K.G., Sheehan, A.F., 1997. Mantle discontinuity structure from midpoint stacks of converted P and S waves across the Yellowstone hotspot track. J. Geophys. Res. 102, 8313–8328.
Fei, Y., Van Orman, J., Li, J., van Westrenen, W., Sanloup, C., Minarik, W., Hirose, K., Komabayashi, T., Walter, M.J., Funakoshi, K., 2004. Experimentally determined postspinel transformation boundary in Mg_2SiO_4 using MgO as an internal pressure standard and its geophysical implications. J. Geophys. Res. 10, B02305. doi:10.1029/2003JB002562.
Flanagan, M., Shearer, P., 1998. Global mapping of topography on transition zone velocity discontinuities by stacking SS precursors. J. Geophys. Res. 103, 2673–2692.
Fukao, Y., Widiyantoro, S., Obayashi, M., 2001. Stagnant slabs in the upper and lower mantle transition region. Rev. Geophys. 39, 291–323.
Govers, R., Wortel, M.J.R., 2005. Lithosphere Tearing at Step Faults: Response to Edges of Subduction Zones, Earth Planet. Sci. Lett. 236, 505–523.
Grand, S.P., 2002. Mantle shear-wave tomography and the fate of subducted slabs. Phil. Trans. R. Soc. A 360, 2475–2491.
Growdon, M.A., Pavlis, G.L., Niu, F., Vernon, F., Rendon, H., 2009. Constraints on mantle flow at the Caribbean-South American plate boundary inferred from shear wave splitting. J. Geophys. Res. 114, B02303. doi:10.1029/2008JB005887.
Higo, Y., Inoue, T., Irifune, T., Yurimoto, H., 2001. Effect of water on the spinel post-spinel transformation in Mg2SiO4. Geophys. Res. Lett. 28, 3505–3508.
Ito, E., Takahashi, E., 1989. Postspinel transformations in the system Mg_2SiO_4-Fe_2SiO_4 and some geophysical implications. J. Geophys. Res. 94, 10637–10646.
Katsura, T., Ito, E., 1989. The system Mg2SiO4-Fe2SiO4 at high pressures and temperatures: precise determination of stabilities of olivine, modified spinel, and spinel. J. Geophys. Res. 94, 15663–15670.
Katsura, T., Yamada, H., Shinmei, T., Kubo, A., Ono, S., Kanzaki, M., Yoneda, Y., Walter, M.J., Ito, E., Urakawa, S., Funakoshi, K., Utsumi, W., 2003. Post-spinel transition in Mg_2SiO_4 determined by high P-T in situ X-ray diffraction. Phys. Earth Planet. Inter. 136, 11–24.
Kennett, B.L.N., Engdahl, E.R., 1991. Travel times for global earthquake location and phase identification. Geophys. J. Int. 105, 429–465.
Kirby, S.H., Stein, S., Okal, E.A., Rubie, D.C., 1996. Metastable mantle phase transformations and deep earthquakes in subducting oceanic lithosphere. Rev. Geophys. 261–306.
Kohlstedt, D.L., Keppler, H., Rubie, D.C., 1996. Solubility of water in the alpha, beta and gamma phases of (Mg, Fe)2SiO4. Contrib. Mineral. Petrol. 123, 345–357.
Lerner-Lam, A.L., Jordan, T.H., 1987. How thick are the continents? J. Geophys. Res. 92, 14007–14026.
Levander, A., Schmitz, M., Lallemant, H.G.A., Zelt, C.A., Sawyer, D.S., Magnani, M.B., Mann, P., Christeson, G., Wright, J.E., Pavlis, G.L., Pindell, J., 2006. Evolution of the Southern Caribbean plate boundary, EOS Trans. AGU 87, 97.
Li, A., Fischer, K.M., Wysession, M.E., Clarke, T.J., 1998. Mantle discontinuities and temperature under the North America. Nature 395, 160–163.
Li, J., Chen, Q.-F., Vanacore, E., Niu, F., 2008. Topography of the 660-km discontinuity beneath northeast China : Implications for a retrograde motion of the subducting Pacific slab. Geophys. Res. Lett. 35, L01302. doi:10.1029/2007GL031658.
Litasov, K., Ohtani, E., Sano, A., Suzuki, A., Funakoshi, K., 2005. Wet subduction versus cold subduction. Geophys. Res. Lett. 32, L13312. doi:10.1029/2005GL022921.
Miller, M., Levander, A., Niu, F., Li, A., 2009. Upper mantle structure beneath the Caribbean – South American plate boundary from surface wave tomography. J. Geophys. Res. 114, B01311. doi:10.1029/ 2007JB005507.
Muirhead, K.J., 1968. Eliminating false alarms when detecting seismic events automatically. Nature 217, 533–534.
Niu, F., Kawakatsu, H., 1995. Direct evidence for the undulation of the 660-km discontinuity beneath Tonga: Comparison of Japan and California array data. Geophys. Res. Lett. 22, 531–534.
Niu, F., Levander, A., Cooper, C.M, Lee, C.-T.A, Lenardic, A., James, D.E, 2004. Seismic constraints on the depth and composition of the mantle keel beneath the Kaapvaal craton, Earth Planet. Sci. Lett. 224, 337–346.
Niu, F., Levander, A., Ham, S., Obayashi, M., 2005. Mapping the subducting Pacific slab beneath southwest Japan with Hi-net receiver functions, Earth Planet. Sci. Lett. 239, 9–17.
Niu, F., Baldwin, T., Pavlis, G., Vernon, F., Rendon, H., Bezada, M., Levander, A., 2007. Receiver function study of the crustal structure of the southeastern Caribbean plate boundary and Venezuela. J. Geophys. Res. 112, B11308. doi:10.1029/2006JB004802.
Pérez, O.J., Bilham, R., Bendick, R., Velandia, J.R., Hernández, N., Moncayo, C., Hoyer, M., Kozuch, M., 2001. Velocity Field across the Southern Caribbean Plate Boundary and Estimates of Caribbean/South-American Plate Motion Using GPS Geodesy 1994–2000. Geophys. Res. Lett. 28 2987-2890.
Polet, J., Anderson, D.L., 1995. Depth extent of cratons as inferred from tomographic studies. Geology 3, 205–208.
Shen, Y., Solomon, S.C., Bjarnason, I.Th., Wolfe, C.J., 1998. Seismic evidence for a lower-mantle origin of the Iceland plume. Nature 395, 62–65.
Vacher, P., Mocquet, A., Sotin, C., 1998. Computation of seismic profiles from mineral physics: the importance of the nonolivine components for explaining the 660 km depth discontinuity. Phys. Earth Planet. Inter. 106, 275–298.
VanDecar, J.C., Russo, R., James, D.E., Ambeh, W.B., Franke, M., 2003. Aseismic continuation of the Lesser Antilles slab beneath continental South America. J. Geophys. Res. 108. doi:10.1029/2001JB000884.
van der Hilst, R.D., Mann, P., 1994. Tectonic implications of tomographic images of subducted lithosphere beneath northwestern South America. Geology 22, 451–454.
van der Hilst, R.D., Widiyantoro, S., Engdahl, E.R., 1997. Evidence for deep mantle circulation from global tomography. Nature 386, 578–584.
van der Meijde, M., Marone, F., Giardini, D., van der Lee, S., 2003. Seismic evidence for water deep in the Earth's upper mantle. Science 300, 1556–1558.
Vidale, J., Benz, H., 1992. Upper-mantle seismic discontinuities and the thermal structure of subduction zones. Nature 356, 678–680.
Wicks, C., Richards, M., 1993. A detailed map of the 660-kilometer discontinuity beneath the Izu-Bonin subduction zone. Science 261, 1424–1427.
Wood, B.J., 1995. The effect of H2O on the 410-kilometer seismic discontinuity. Science 268, 74–76.

Further reading

Tajima, F., Grand, S.P., 1998. Variation of transition zone high velocity anomalies and depression of the "660"km discontinuity associated with subduction zones from the southern Kuriles to Izu-Bonin. J. Geophys. Res. 103, 15015–15036.